Geomechanics and Engineering, *Vol. 22, No. 2 (2020) 153-163*
DOI: https://doi.org/10.12989/gae.2020.22.2.153

Infiltration characteristics and hydraulic conductivity of weathered unsaturated soils

Young-Suk Song[1a] and Seongwon Hong[*2]

[1]*Geologic Environment Division, Korea Institute of Geoscience and Mineral Resources, Daejeon 34132, Korea*
[2]*Department of Safety Engineering, Korea National University of Transportation, Chungju-si, Chungbuk 27469, Korea*

(Received September 29, 2019, Revised February 21, 2020, Accepted June 12, 2020)

Abstract. Laboratory experiments were conducted with two different soil conditions to investigate rainfall infiltration characteristics. The soil layer materials that were tested were weathered granite soil and weathered gneiss soil. Artificial rainfall of 80 mm/hr was reproduced through the use of a rainfall device, and the volumetric water content and matric suction were measured. In the case of the granite soil, the saturation velocity and the moving direction of the wetting front were fast and upward, respectively, whereas in the case of the weathered gneiss soil, the velocity and direction were slow and downward, respectively. Rainfall penetrated and saturated from the bottom to the top as the hydraulic conductivity of the granite soil was higher than the infiltration capacity of the artificial rainfall. In contrast, as the hydraulic conductivity of the gneiss soil was lower than the infiltration capacity of the rainfall, ponding occurred on the surface: part of the rainfall first infiltrated, with the remaining rainfall subsequently flowing out. The unsaturated hydraulic conductivity function of weathered soils was determined and analyzed with matric suction and the effective degree of saturation.

Keywords: infiltration; rainfall intensity; unsaturated hydraulic conductivity; weathered gneiss soil; weathered granite soil

1. Introduction

Water on the surface can enter soils through a process called infiltration (Philip 1957). Infiltration resulting from the force of gravity and capillary action can influence the temporal and spatial conditions of subsurface hydrologic processes and geotechnical properties. For example, if a perched water table is developed via rainfall, it results in increased main groundwater level, pore water pressure, and unit weight of the soil. Infiltration is a function of roughness, stoniness, slope angle, porosity, voids, vegetation, surface crust, topsoil structure, rainfall, raindrop impact, and biological activity (Poesen 1984, Bradford *et al.* 1987, Wilson and Luxmoore 1988, Poesen *et al.* 1990, Dunne *et al.* 1991, Valentin and Bresson 1992, Mwendera and Feyen 1994, Leonard and Andrieux 1998). These factors are strongly interconnected and interrelated, and thus it is extremely difficult to study all of the factors at once when investigating soil infiltration. In general, one or two factors are considered for field observation and laboratory tests, and analytical and numerical infiltration relationships have been proposed and developed to understand the infiltration characteristics of unsaturated soils.

Soil infiltration depends on rainfall and raindrops. Field tests have shown that the primary factor that reduces infiltration rate is crust formation influenced by raindrop impact (Morin and Benyamini 1977, Beven and Germann, 1982). Romkens *et al.* (1986) studied the effects of raindrops on ponding and infiltration and reached the conclusion that raindrops destroy and reconstruct soil particle arrangement, resulting in a reduction in the infiltration rate. Abu-Awwad (1997) performed a field test to study water infiltration and redistribution in soils as influenced by surface crust and concluded that the use of sand columns without soil ridges results in increased amounts of moisture in the soil layer and a reduction in surface runoff. Schindewolf and Schmidt (2012) found that soil infiltration is inversely proportional to cumulative rainfall from experiments using a runoff feeding device.

In addition to rainfall and raindrops, soil infiltration is dependent on both rainfall intensity and the hydraulic conductivity of unsaturated soils. In 1958, McIntyre found that the permeability of surface soils was 2,000 times less than that of underlying soils through field observation. Azooz and Arshad (1996) carried out field experiments to investigate soil infiltration and hydraulic conductivity under long-term no-tillage and conventional tillage systems, and it was found that unsaturated hydraulic conductivity increases with matric potential. Foley and Silburn (2002) studied the effects of rainfall intensity, drop size, and impact frequency on steady state flow for sealed soils and observed that infiltration rates increased with increasing rainfall intensity. In 2006, Hawke *et al.* performed laboratory tests to study the permeability coefficient at the surface under various rainfall intensity conditions, concluding that rainfall intensity significantly affects hydrological conductivity. Mahmood *et al.* (2012) investigated the effects of

*Corresponding author, Assistant Professor
E-mail: shong@ut.ac.kr
[a]Principal Researcher

ISSN: 2005-307X (Print), 2092-6219 (Online)

anisotropic hydraulic conductivity on suction stress and proposed a reliability index for an unsaturated soil under uniform rainfall. To investigate the relationship between infiltration velocity and rainfall conditions, Park *et al.* (2011) conducted unsaturated soil column tests with weathered granite soil and weathered gneiss soil. It was concluded that the effects of reduced matric suction results from the reduction of air in the soil structure. Correlations between the hydraulic conductivity of geosynthetic clay liners and the physico-chemical properties of bentonites were investigated by Ören *et al.* (2018). This study found that the hydraulic conductivity of geosynthetic clay liners was related to the final height and final water content.

Through field and laboratory experiments, many researchers and scholars have proposed several infiltration models. Mein and Larson (1973) developed the simple two-state infiltration model, which is a function of soil properties, initial moisture content, and rainfall intensity. In 1997, the dynamics sealing model was developed by Assouline and Mualem to study how infiltration was affected by rainfall intensity, the second moment of the drop-size density distribution, the maximal drop diameter, the compaction limit of the given soil, and its initial shear strength. Based on the effective stress principle, Lu and Griffiths (2004) developed a quantitative method of determining the profiles of suction stress in unsaturated soils under steady-state flow rate in the infiltration form. In 2013, Zhan *et al.* proposed an analytical solution for rainfall infiltration in infinite slopes based on the general partial differential equation with water flow through unsaturated soil. Ojha *et al.* (2017) proposed analytical formulations based on effective saturated hydraulic conductivity and the Green-Ampt model to estimate field-scale infiltration rates.

In spite of the contributions of the aforementioned studies, the relationship between rainfall intensity and the hydraulic conductivity of different soil types has yet to be clearly defined. Therefore, there is a fundamental need for additional experimental investigations to understand soil infiltration characteristics. In this study, laboratory tests were performed to study the rainfall infiltration features of soil layers composed of weathered granite soil or weathered gneiss soil under constant rainfall intensity. In the experiment, changes in the volumetric water content and matric suction were measured, and the saturation pattern was thoroughly observed and analyzed. Based on the experimental results, the correlation between rainfall intensity and hydraulic conductivity was analyzed, and the saturation condition in the soil layer due to rainfall was experimentally identified.

2. Experimental setup

2.1 Test apparatus

Model tests were conducted to understand the rainfall infiltration characteristics of weathered soils. Fig. 1(a) shows a schematic diagram of the rainfall infiltration system consisting of a soil box, rainfall simulation equipment, and instrumentation devices. The soil box was connected to a valve and a balance to measure the amount of rainfall that does not infiltrate into the soil layers. The rainfall simulation apparatus was composed of a sprinkler, a rainfall intensity controller, and a water supply tank. The rainfall intensity controller consisted of two peristaltic pumps and was used to supply water constantly to the sprinkler, which was composed of needles. The instrumentation devices consisted of time domain reflectometry (TDR) sensors (EC-5, Decagon Devices, Inc.), tensiometers (2100F, Soilmoisture Equipment Corp.), a data logger (CR 1000, Campbell Scientific, Inc.), and a computer. The volumetric water content and matric suction values were recorded using the TDR and tensiometers, respectively, and were installed at various depths. A panoramic view of the rainfall infiltration test apparatus is shown in Fig. 1(b). Fig. 1(c) illustrates the locations of the sensors in the soil box. The dimensions of the soil container box were as follows: 600 mm in length, 150 mm in width, and 560 mm in height. The box was made with transparent acrylic plates of 10 mm thickness to observe the behavior of rainfall infiltration within the soil layer. The actual dimensions of the soil layer installed during the experiment were as follows: 600 mm in length, 150 mm in width, and 500 mm in height. Based on the fact that the experiment was a soil element test, the dimensions of the soil layer were determined and it was assumed that no scale effects existed. In addition, the soil box was designed based on the topographic characteristics of natural slopes in Korea, where the surface depth is shallow and the soil layer is located on the bedrock; thus, a no-flow boundary was present at the bottom of the box. The soil box was designed to be able to install TDR sensors and tensiometers, and the depths of the sensors were 100, 250, and 400 mm from the top of the box. A total of six sensors (three TDR and three tensiometers) were located horizontally at a distance of 100 mm from the edge of the soil box to the center to reduce the influence of the sensors on the ground condition and rainfall infiltration. The volumetric water content and the matric suction data were automatically recorded every 5 seconds, transmitted to the data logger, and subsequently stored on the computer. The sprinkler had needles, each with a diameter of 1 mm; the needles were installed at a constant interval of 45 mm × 45 mm. The distance between the soil surface and the end of the needles was determined as 60 mm to minimize the disturbance of the soil caused by the artificial rainfall. The sprinkler was connected to two peristaltic pumps and was designed to constantly supply rainfall. The peristaltic pumps were of the model BT 100M from Baoding Shenchen Precision Pump Co., Ltd, with each pump having a flow rate of 0.1-100 rpm. The system was made to control the rainfall intensity through a combination of the two pumps.

An automatic measuring device for soil-water characteristic curves (SWCC) developed by Song *et al.* (2012b) was employed. As the experimental results were automatically measured by the system, human error was minimized. The device consisted of a flowcell, pressure regulator, water reservoir, air bubble trap, balance, shelf, and storage box. Both the drying and wetting processes were reenacted by applying air pressure and by injecting water to the specimen, respectively. The maximum air pressure was 300 kPa and a high-air-entry disk with a

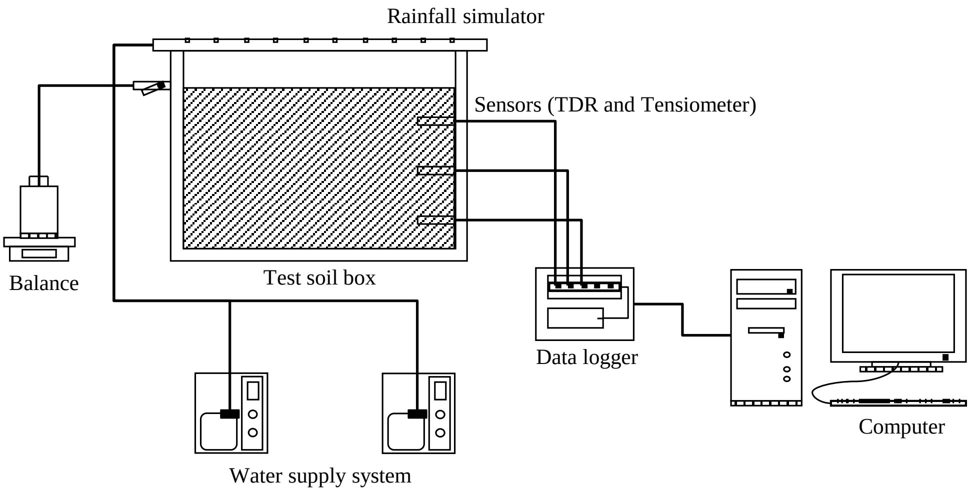

(a) Schematic diagram

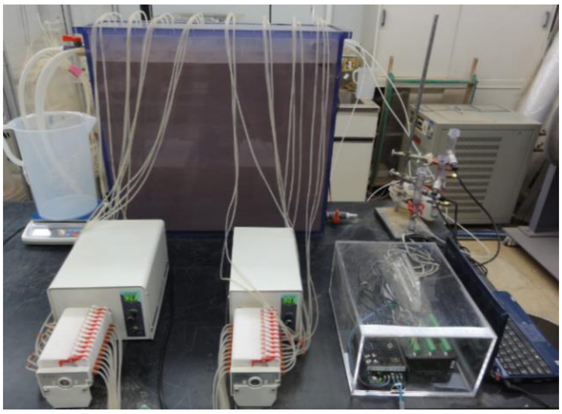

(b) Panoramic view

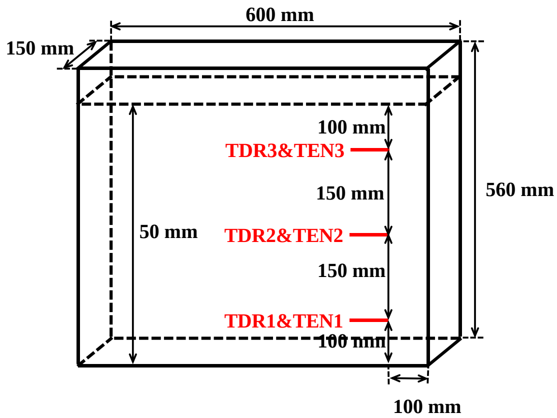

(c) Location of the sensors in the soil box

Fig. 1 Rainfall infiltration test: (a) schematic diagram, (b) panoramic view and (c) location of the sensors in the soil box

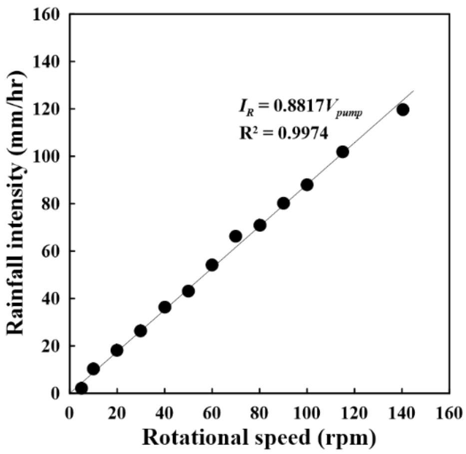

Fig. 2 Estimation of rainfall intensity according to the pump rotational speed

pressure of 3 bars was employed to prevent the flow of pore air and soil particles.

2.2 Estimation of rainfall intensity

Preliminary tests were performed to simulate specific rainfall intensities using the rainfall simulation equipment that was designed to reproduce various rainfall intensities.

As the amount of water supplied to the sprinkler varies according to the rotational speeds of the two peristaltic pumps, the amount of artificial rainfall was measured while increasing the rotational speeds of the pumps. The rotational speeds of the two pumps were made equal at this moment. The experimental procedure was as follows; the amount of rainfall for 30 minutes was measured under the condition of a specific rotational speed and was subsequently converted into rainfall intensity. Artificial rainfall intensity was determined according to a variety of rotational speeds of the peristaltic pumps. Fig. 2 presents the estimation of rainfall intensity as a function of the rotational speed. The rainfall intensity linearly increased with the pump rotational speed, and the linear regression equation was determined, as shown in Eq. (1). This was used to simulate specific rainfall intensities in the model test. For example, if a rainfall intensity of 80 mm/hr was to be reproduced, the pump rotational speed was adjusted to approximately 90 rpm.

$$I_R = 0.8817V_{pump}. \tag{1}$$

where I_R is the artificial rainfall intensity and V_{pump} is the rotational speed of the two pumps.

3. Ground model

3.1 Ground materials

The weathered granite soil and weathered gneiss soil consisted of Jumunjin sand, which is the Korean Standard Sand, and field soil from Yongin in South Korea, respectively. Various soil tests were conducted to investigate the physical properties of the soil samples. Table 1 provides the results of the soil tests. The particle size distribution curves of the granite soil and the gneiss soil are simultaneously plotted in Fig. 3. Poorly graded granite and well-graded gneiss soils were clearly observed.

3.2 Test description

To investigate rainfall infiltration characteristics of soils according to soil type, two different soil conditions, namely weathered granite soil and weathered gneiss soil, were employed under the same rainfall intensity of 80 mm/hr. The test procedure was as follows; 1) weathered granite soil and weathered gneiss soil were placed in an oven and dried at 105 °C for more than 24 hours, 2) the dried soil samples formed 3 layers due to the installation of the instruments, and the relative density and unit weight was adjusted by using compaction equipment and a rubber hammer, 3) the TDR and tensiometers were installed together while forming the soil layers, and the sensors were placed at 100, 250, and 400 mm from the top of the box, 4) the sprinkler was installed on the upper part of the test box and was then connected to the peristaltic pump using tubes, 5) the rotational speed of the peristaltic pump was controlled to conduct the tests under a specific rainfall intensity of 80 mm/hr, 6) the volumetric water content and matric suction were measured through the TDR and tensiometers, respectively, which were subsequently recorded on the computer, 7) rainfall infiltration characteristics such as saturation velocity and trend were analyzed using the observed volumetric water content and matric suction. The results were compared with hydraulic conductivity.

Table 1 Physical properties of the weathered granite and weathered gneiss soils

Description	Symbol	Granite soil	Gneiss soil
Specific gravity	G_s	2.621	2.714
Dry density	γ_d (g/cm^3)	1.543	1.221
Effective particle size	D_{10} (mm)	0.420	0.001
D_{30} particle size	D_{30} (mm)	0.500	0.032
D_{60} particle size	D_{60} (mm)	0.600	0.470
Uniformity coefficient	C_u	1.4	470.0
Coefficient of curvature	C_c	1.0	2.2
Soil classification	USCS	SP	SM

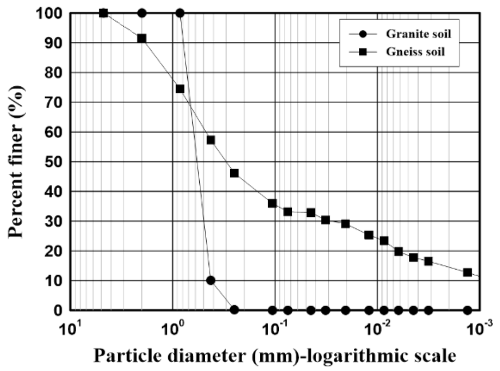

Fig. 3 Particle size distribution curves of the weathered granite and gneiss soils

4. Experimental results

4.1 Weathered granite soil

Fig. 4(a) depicts the experimental results of rainfall infiltration for the granite soil. In order to compare volumetric water content and matric suction in the same figure, the experimental data obtained from the TDR and tensiometers were plotted together. Solid and dashed lines were used to represent the volumetric water content and matric suction, respectively, as shown in Fig. 4(a). Similar trends were clearly observed between volumetric water content and matric suction. There was a signal delay between the matric suction and volumetric water content data as the former was collected after the volumetric water content reached a certain point. In addition to the delay, although the artificial rainfall water passed through the soil layer, the sensors TDR 2&3 and TEN 2&3 did not receive any signals of water flow. This was primarily due to the fact that the water must stay in the pores for the sensors to work, but it instead passed through the sensors, and so the raw data for volumetric water content and matric suction were not recorded. The initial matric suction of the granite soil was in the range of 20-23 kPa and reached 0 kPa as saturation was achieved. The volumetric water content of the granite soil was 0% in the early stages due to the use of dried soil; subsequently, it reached approximately 30% as it became fully saturated.

Fig. 4(b) shows the saturation condition of the granite soil due to the artificial rainfall. In the infiltration model tests on granite soil, a wetting front was formed from the bottom of the box and the saturation direction was upward. As the hydraulic conductivity of the granite soil was relatively large, it was believed that the infiltration water could not stay on the surface of the soil and moved to the bottom.

4.2 Weathered gneiss soil

Fig. 5(a) depicts the test data of rainfall infiltration for the gneiss soil under a rainfall intensity of 80 mm/hr. The initial matric suction of the gneiss soil was between 70 kPa and 80 kPa and reached 0 kPa as the soil became saturated. As the soil was progressively saturated, the matric suction (or negative pore pressure) started to decrease until volumetric water content began to increase. The decrease in matric suction at the beginning of the experiment was due to the fact that the gneiss soil originally had a lower matric suction; as such, the matric suction decreased when the soil

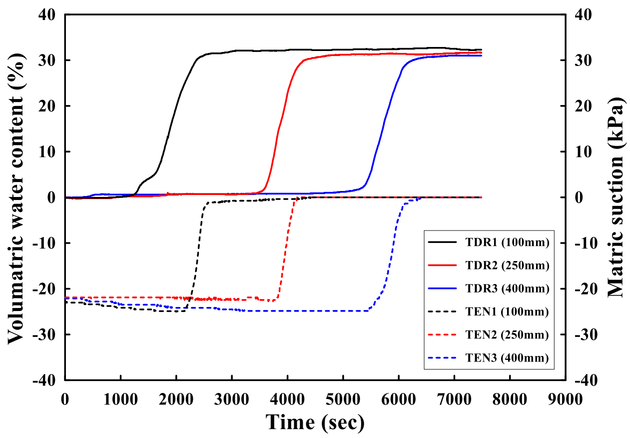

(a) Volumetric water content and matric suction

(b) Saturation condition due to rainfall infiltration

Fig. 4 Experimental results of rainfall infiltration on weathered granite soil: (a) volumetric water content and matric suction and (b) saturation condition due to rainfall infiltration

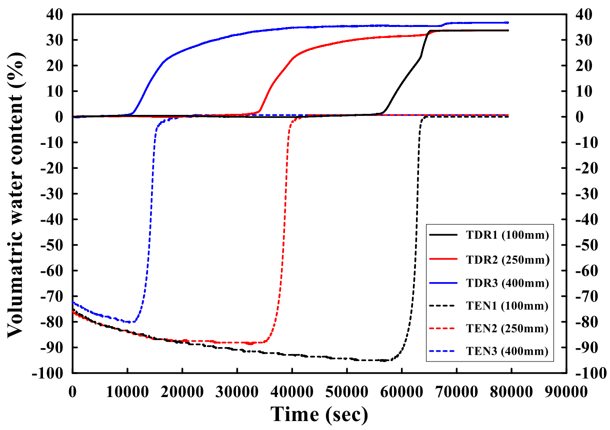

(a) Volumetric water content and matric suction

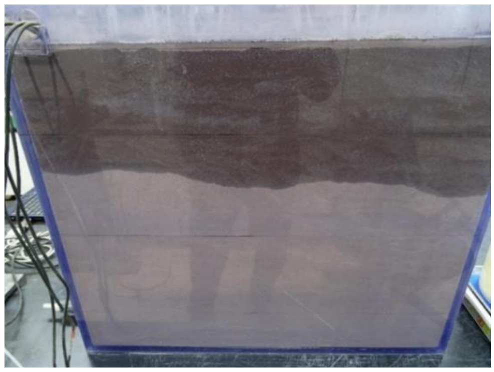

(b) Saturation condition due to rainfall infiltration

Fig. 5 Experimental results of rainfall infiltration on weathered gneiss soil: (a) volumetric water content and matric suction and (b) saturation condition due to rainfall infiltration

was partially saturated and then sharply increased under saturated conditions. The significantly higher matric suction compared to the weathered granite soil was considered to be caused by the presence of a large amount of fine-grained soil in the gneiss soil sample. The initial water content of the gneiss soil was 0% as it was dried for more than 24 hours, and the water content reached approximately 30% as saturation was achieved. Under the condition of 80 mm/hr rainfall intensity, it took approximately 6,500 seconds to fully saturate the soil layers of the granite soil from the bottom to the sensors TDR3 and TEN3, as shown in Fig. 1(c), whereas for the gneiss soil, approximately 65,000 seconds was required to saturate the soil layers from the top to the sensors TDR1 and TEN1, as shown in Fig. 1(c)). Therefore, in the case of the gneiss soil, the time to fully saturate the entire soil layer was approximately ten times greater than the granite soil.

Fig. 5(b) shows the saturation condition of the weathered gneiss soil caused by rainfall infiltration. The saturation area began at the surface and proceeded to the bottom of the soil layer. In the case of the gneiss soil, it was found that the wetting front started at the top of the box and the soil was saturated in a downward direction. As the hydraulic conductivity of the gneiss soil was relatively low, the infiltration water could not fully penetrate into the soil and ponding occurred on the surface of the soil. Thus, the wetting front descended and the soil layer became fully saturated.

Table 2 Curve-fitting parameters of the weathered granite and the weathered gneiss soils

Type	Path	α (kPa^{-1})	n	m	R^2
Granite Soil	Drying	0.393	8.553	0.883	0.995
	Wetting	0.593	5.561	0.820	0.984
Gneiss soil	Drying	0.299	2.018	0.504	0.994
	Wetting	0.846	1.601	0.375	0.996

4.3 Unsaturated characteristics

Data such as the matric suction and volumetric water content of the weathered granite soil and weathered gneiss soil were collected from the automatic measuring device and were analyzed with the model proposed by van Genuchten (1980) to determine the SWCCs for the given conditions. The equation is as follows:

$$S_e = \frac{S - S_r}{1 - S_r} = \frac{\theta - \theta_r}{\theta_s - \theta_r} = \left(\frac{1}{1 + [\alpha h]^n}\right)^m \tag{2}$$

where S_e is the effective degree of saturation, S_r is the residual degree of saturation, θ_s is the saturated value of the

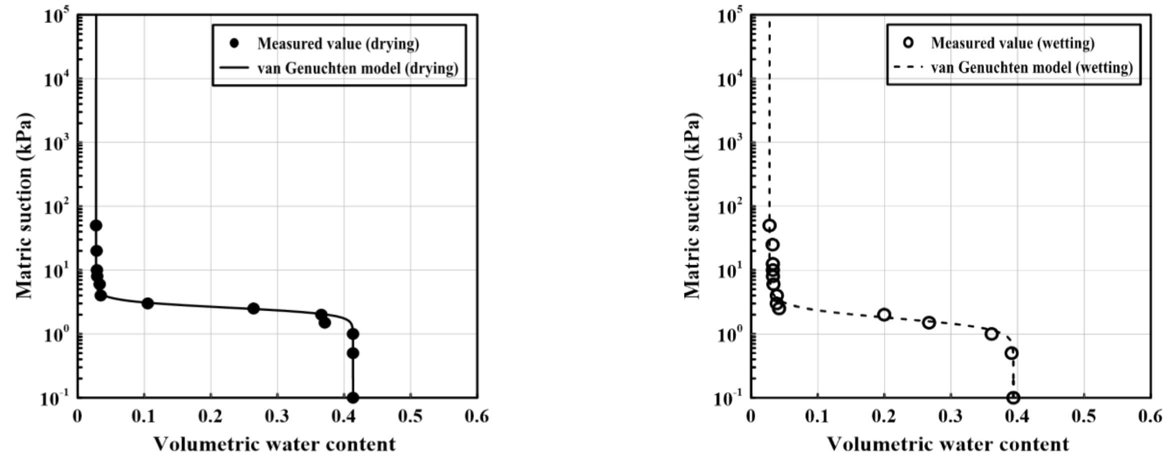

(a) Weathered granite soil

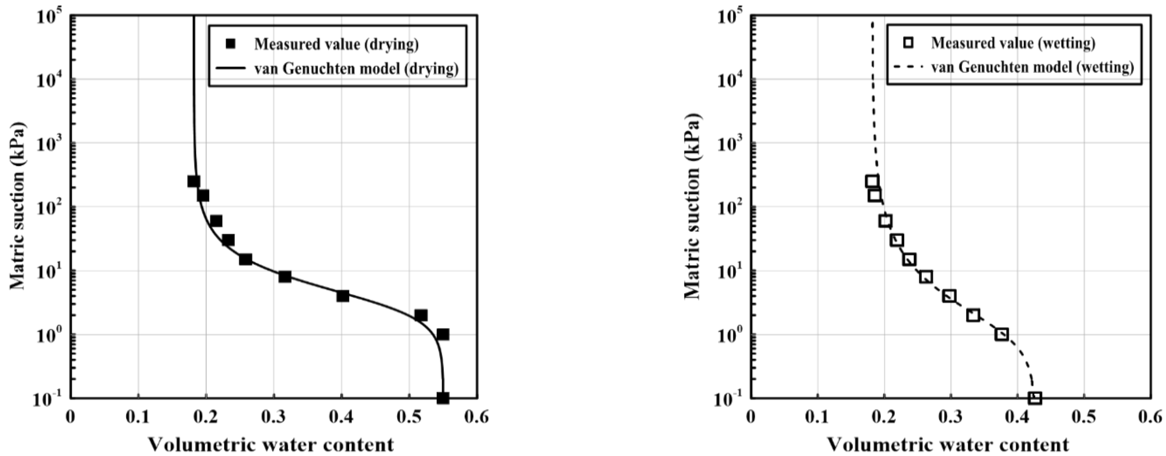

(b) Weathered gneiss soil

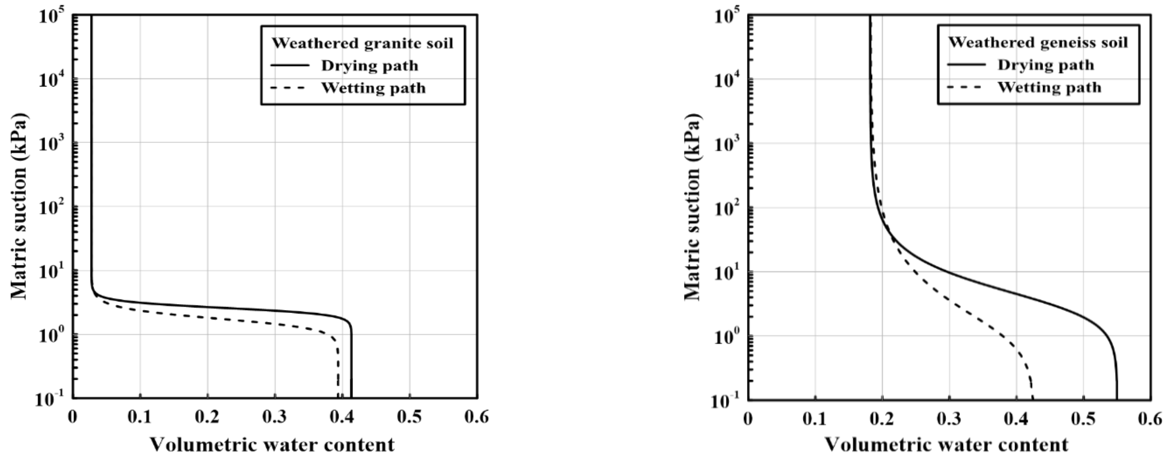

(c) Hysteresis during drying and wetting paths

Fig. 6 Soil-water characteristic curve: (a) weathered granite soil, (b) weathered gneiss soil and (c) hysteresis during drying and wetting paths

soil-water content, θ_r is the residual value of the soil-water content, α is a parameter related to the air-entry value, h is the matric suction (difference between pore air pressure and pore water pressure (u_a-u_w)), n is a parameter related to the slope of the SWCC, and m is a parameter related to the residual water content. The fitting parameters (α, n, and m) were determined for the granite soil with a relative density of 75% and the gneiss soil by employing nonlinear least square analysis between the matric suction and volumetric water content, and is summarized in Table 2.

Fig. 6 shows the SWCC determined by the van Genuchten equation for the drying and wetting paths. Nonlinear curves were observed and the slope of the relationship between matric suction and volumetric water content were all different. Fig. 6(a) and 6(b) display the SWCCs for the weathered granite soil with a relative density of 75% and the weathered gneiss soil, respectively. For both soils, the volumetric water content during the drying path was measured as relatively higher than that during the wetting path for the same matric suction, which is referred to as hysteresis behavior, as demonstrated in Fig. 8(c). In case of the granite soil, a relatively large variation in the volumetric water content occurred under a small range of matric suction, whereas a small variation in the volumetric water content was observed according to matric suction for the gneiss soil. Moreover, under the same condition of volumetric water content, the field capacity of matric suction for the gneiss soil was measured as larger than that in the case of the granite soil. The primary reason for this was that the granite soil had uniform particle size, whereas the gneiss soil contained silty components.

5. Results and discussion

Fig. 7 shows the saturation velocity of the soil layer with depth and time. The saturation velocity was defined as a ratio of the thickness of the soil layer where the instrumentation devices were placed to the time at which the measured data converged to certain values, signifying that the soil was fully saturated at that depth. For example, in the case of the weathered granite soil, it took 2,520 seconds to fully saturate the soil region at a depth of 100 mm, and thus the saturation velocity was determined to be 3.97×10^{-2} mm/sec. The saturation velocity of the granite soil was noticeably faster than that of the gneiss soil as the hydraulic conductivity of the former was higher than that of the latter. On the other hand, the slow saturation velocity of the weathered gneiss soil was relatively maintained with depth and time, whereas the weathered granite soil demonstrated increasing trends in saturation velocity with depth and time.

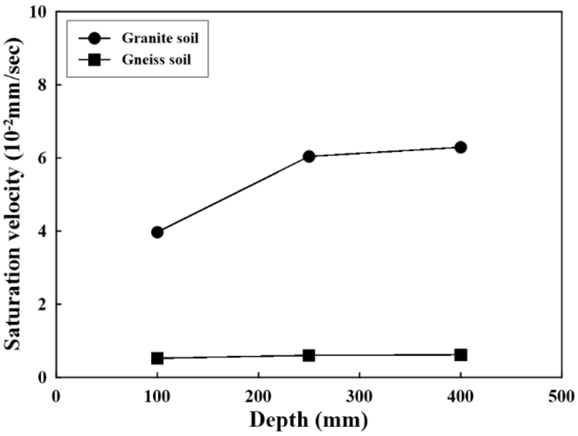

(a) Depth

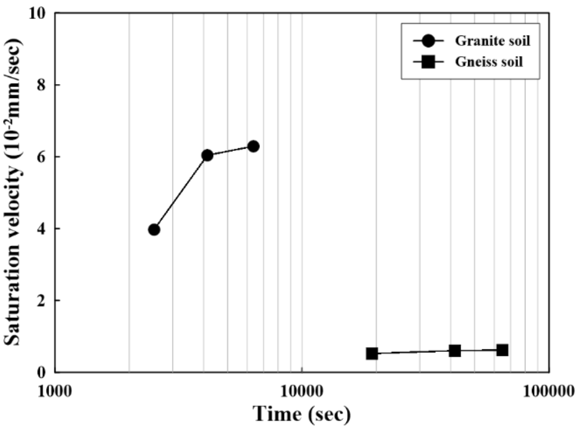

(b) Time

Fig. 7 Saturation velocity with depth and time: (a) dept and (b) time

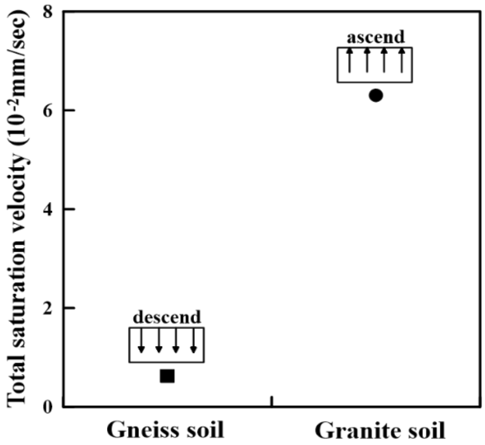

Fig. 8 Total saturation velocity of all soil layers

Fig. 8 shows the total saturation velocity, which was calculated as a ratio between a soil layer thickness of 400 mm and the time elapsed to fully saturate the soil area. The total saturation velocity was relatively faster for the granite soil than that of the weathered gneiss soil due to its uniform particle size distribution (referred to as poorly graded) and the small amount of fine-grained soil. In contrast, as the particle size distribution was well-graded and a large amount of fine-grained soil was present in the gneiss soil, the total saturation velocity was found to be slower than that of the weathered granite soil.

5.2 Saturation trends according to depth

Fig. 9(a) displays the variation in volumetric water content over time in the weathered granite soil layer. After 1 hour of rainfall infiltration, the volumetric water content reached 0.8, 2.2, and 32.1% at depths of 100, 250, and 400 mm, respectively. The time required to fully saturate the granite soil layer via upward infiltration was approximately two hours and four minutes of the rainfall.

The change in volumetric water content of the weathered gneiss soil with depth and time is shown in Fig. 9(b). No significant change was observed until 3 hours after the initial rainfall infiltration. Moreover, after approximately ten hours of rainfall infiltration, changes in the volumetric water content began to appear at a depth of 250 mm, whereas at a depth of 400 mm, changes in volumetric water content began to appear after approximately seventeen hours of rainfall infiltration. It took approximately twenty-two hours for the entire soil layer to be saturated from the surface to the bottom of the soil layer. This is equivalent to a time that is eleven times the full saturation time of the granite soil under the same rainfall intensity.

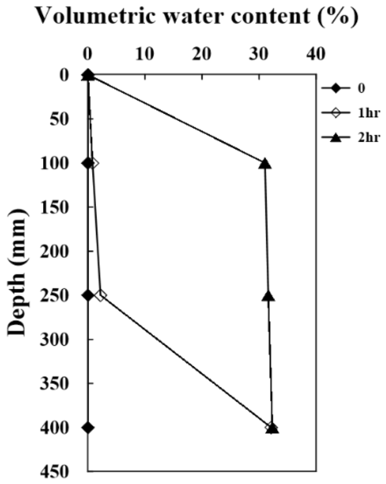

(a) Weathered granite soil

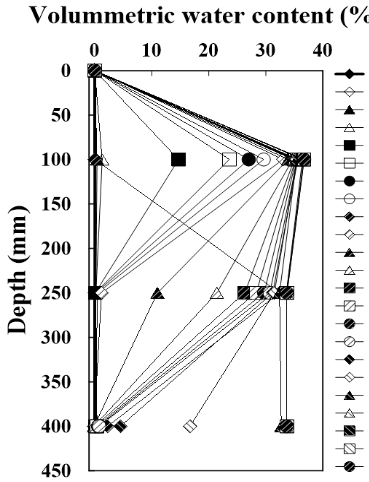

(b) Weathered gneiss soil

Fig. 9 Variation in the volumetric water content with depth and time: (a) weathered granite soil and (b) weathered gneiss soil

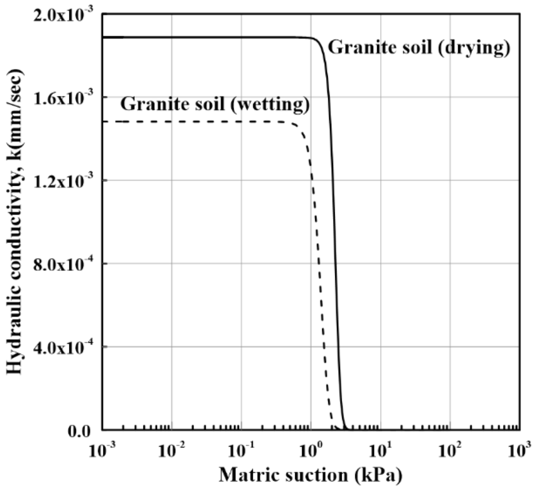

(a) Matric suction (granite)

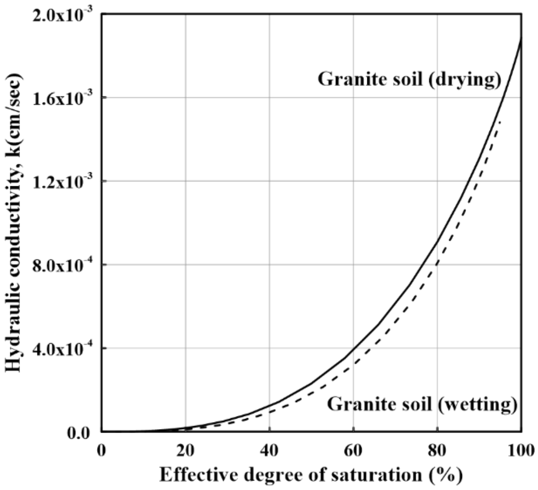

(b) Effective degree of saturation (granite)

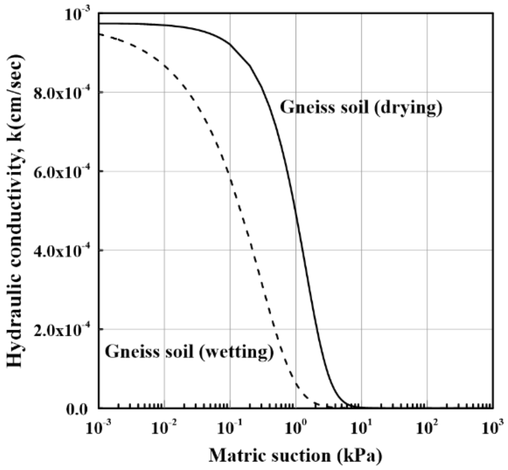

(c) Matric suction (gneiss)

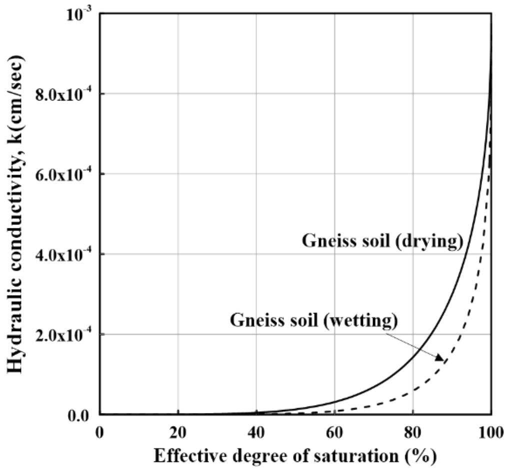

(d) Effective degree of saturation (gneiss)

Fig. 10 Hydraulic conductivity functions of weathered soil; (a) matric suction (granite), (b) effective degree of saturation (granite), (c) matric suction (gneiss) and (d) effective degree of saturation (gneiss)

5.3 Correlation between rainfall infiltration and hydraulic conductivity

Kim *et al.* (1991) proposed that, when rainfall infiltrates into the ground, a wetting front is formed in unsaturated soils and that the infiltration behavior completely depends on rainfall intensity. In particular, the rate of the formation of the wetting front increased with an increase in rainfall

Table 3 Hydraulic conductivity of the weathered granite and the weathered gneiss

Condition	Hydraulic conductivity (mm/sec)
Granite soil	1.88×10^{-2}
I = 80 mm/hr	2.22×10^{-3}
Gneiss Soil	9.47×10^{-4}

intensity when rainfall intensity was less than five times the hydraulic conductivity. If the rainfall intensity is greater than five times the hydraulic conductivity, the process speed of the wetting front is no longer dependent on rainfall intensity. Therefore, it was suggested that the maximum rainfall intensity should be less than five times the hydraulic conductivity of the soil for infiltration into soil layers via rainfall. Song *et al.* (2012a) estimated the intensity of rainfall that infiltrated into soil layers based on field measurements and numerical analysis results in the process of analyzing the deformation behavior of stabilizing piles installed on slopes. The hydraulic conductivity in the saturated soil and the rainfall intensity were observed as 2.80×10^{-3} mm/sec and 10.08 mm/hr, respectively. Therefore, when rainfall intensity is equal to or lower than the hydraulic conductivity of the soil layer, rainfall is able to easily infiltrate the soil. Under rainfall intensities greater than the hydraulic conductivity, it was proposed that the rainfall does not infiltrate properly and flows out to the surface.

In this study, to measure the hydraulic conductivity of the saturated soil sample, the permeation method using the triaxial compression test system according to ASTM-D5084 (2016) was employed. The test method aimed to measure the flow rate and the time of discharge by applying a constant water pressure to the inside of the soil sample after forming and saturating it. Table 3 provides the measured hydraulic conductivity values of the granite and gneiss soils for the wetting process, as the focus of this study was rainfall infiltration. The hydraulic conductivity values of the granite and gneiss soils were 1.88×10^{-2} mm/sec and 9.47×10^{-4} mm/ sec, respectively. A rainfall intensity of 80 mm/hr can be converted to 2.22×10^{-3} mm/sec.

Comparison of the hydraulic conductivity of the granite soil and the artificial rainfall intensity indicated that the former was higher than the latter, and so the rainfall infiltrated into the bottom of the soil layer and the saturation started from the bottom of the box. In the case of the gneiss soil, as the hydraulic conductivity was lower than the rainfall intensity, the rainfall did not infiltrate directly into the ground, resulting in the outflow phenomenon and saturation to begin at the surface of the soil layer. In other words, in the case of the granite soil, which had a higher hydraulic conductivity than the rainfall intensity, the saturation progressed via the increase of groundwater level during rainfall, whereas in the case of the gneiss soil, which had a lower hydraulic conductivity than the rainfall intensity, the wetting front was formed at the surface and the saturation region progressed downward. Furthermore, the findings regarding the correlation between hydraulic conductivity and rainfall intensity confirms the experimental results. This is the primary reason why a rainfall intensity of 80 mm/hr was selected for the experiment.

Fig. 10 shows the hydraulic conductivity functions of the weathered granite and the weathered gneiss soils, respectively. van Genuchten (1980) proposed the model for the hydraulic conductivity function of unsaturated soils as follows:

$$K(h) = K_s \frac{\left[1-(\alpha h)^{n-1}\left(1+(\alpha h)^n\right)^{-m}\right]^2}{\left[1+(\alpha h)^n\right]^{m/2}} \tag{3}$$

$$K(\mathrm{S}_e) = K_s \cdot S_e^{1/2}\left[1-\left(1-S_e^{1/m}\right)^m\right]^2 \tag{4}$$

where α is a parameter related to the air-entry value, h is the matric suction (difference between pore air pressure and pore water pressure), n is a parameter related to the slope of the SWCC, m is a parameter related to the residual water content, K_s is the saturated hydraulic conductivity and S_e is the effective degree of saturation. The fitting parameters (α, n, and m) were used from Table 2 and saturated hydraulic conductivity (K_s) was obtained according to ASTM-D5084. Fig. 10(a) presents the hydraulic conductivity of the granite soil as a function of matric suction. It was clear that the unsaturated hydraulic conductivity was constant at the beginning for the drying and wetting processes and dramatically decreased immediately before applying the air for the drying path or the water for the wetting path. The drying process exhibited higher hydraulic conductivity compared to the wetting process at the same matric suction level, which was similar to the SWCC. In addition, the drying process exhibited hysteresis. The hydraulic conductivity of the granite soil is plotted in Fig. 10(b) as a function of effective degree of saturation. The drying process exhibited a higher hydraulic conductivity compared to the wetting process at the same effective degree of saturation. Fig. 10(c) shows the hydraulic conductivity of the gneiss soil as a function of matric suction. The hydraulic conductivity was initially constant and then decreased with matric suction for both the drying and wetting processes. For the drying and wetting paths, exponential growth curves were calculated for hydraulic conductivity as the effective degree of saturation increased, as presented in Fig. 10(d). The hydraulic conductivity of the granite soil was determined to be slightly higher than that of the gneiss soil at the same effective degree of saturation.

6. Conclusions

In this research, a model experiment was carried out to understand rainfall infiltration characteristics in soil layers according to the soil type and rainfall intensity. Weathered granite soil and weathered gneiss soil were used to form the soil layers for the tests. The volumetric water content and matric suction were observed under the condition of 80 mm/hr of artificial rainfall. Based on the test results, the correlation between the hydraulic conductivity of the soil and rainfall intensity was analyzed, the unsaturated hydraulic conductivity was determined, and the following conclusions were drawn:

- The saturation velocity of the granite soil was fast and increased with both depth and time due to the uniform particle size distribution and the small amount of fine-grained soil. In contrast, the saturation velocity of the gneiss soil was slow and independent of depth and time due to the well-graded soil and the large amount of fine-grained soil included in the soil materials. In addition, the direction of saturation progressed from the bottom to the top for the granite soil, whereas the saturation of the gneiss soil began at the surface of the soil layer and descended.

- Approximately two hours were required to fully saturate the soil layers of the granite soil, whereas approximately twenty-two hours were required to saturate the gneiss soil from the top to the bottom. The main reason for these observations was due to the weathered granite and gneiss soils having high and low hydraulic conductivity, respectively.

- Analysis of the correlation between rainfall infiltration according to rainfall intensity and hydraulic conductivity showed that the hydraulic conductivity of the granite soil was higher than the rainfall intensity; as a result, all of the rainfall penetrated into the ground and the direction of the saturation was upward. In contrast, in the case of the gneiss soil, as the rainfall intensity was higher than the hydraulic conductivity, ponding occurred on the ground surface and only a part of the rainfall penetrated into the soil, with the rest flowing out from the ground surface. As a result, the saturation region progressed downward to the bottom of the box.

- The unsaturated hydraulic conductivities of the granite and gneiss soils was determined by using the van Genuchten model and were expressed as functions of matric suction or effective degree of saturation. Depending on the soil conditions and type, the patterns of rainfall infiltration vary and the degree of saturation of the soil layers varies accordingly. As the hydraulic conductivity of unsaturated soils change according to the degree of saturation of the soil layers, unsaturated hydraulic conductivity changes with rainfall intensity, influencing rainfall infiltration in soil layers.

Acknowledgments

This research was supported by the Basic Research Project (Grant No. 20-3412-1) of the Korean Institute of Geoscience and Mineral Resources (KIGAM) funded by the Ministry of Science and ICT of Korea. The authors thank Chul-Min Kim for his valuable collaboration during the experiments. The views expressed are those of authors, and do not necessarily represent the sponsors.

References

Abu-Awwad, A.M. (1997), "Water infiltration and redistribution within soils affected by a surface crust", *J. Arid Environ.*, **37**(2), 231-242. https://doi.org/10.1006/jare.1997.0280.

Assouline, S. and Mualem, Y. (1997), "Modeling the dynamics of seal formation and its effect on infiltration as related to soil and rainfall characteristics", *Water Resour. Res.*, **33**(7), 1527-1536. https://doi.org/10.1029/96WR02674.

ASTM-D5084 (2016), *Standard Test Methods for Measurement of Hydraulic Conductivity of Saturated Porous Materials Using a Flexible Wall Permeameter*, ASTM International, West Conshohocken, Pennsylvania, U.S.A.

Azooz, R.H. and Arshad, M.A. (1996), "Soil infiltration and hydraulic conductivity under long-term no-tillage and conventional tillage systems", *Can. J. Soil Sci.*, **76**(2), 143-152. https://doi.org/10.4141/cjss96-021.

Beven, K. and Germann, P. (1982), "Macropores and water flow in soils", *Water Resour. Res.*, **18**(5), 1325-1331. https://doi.org/10.1029/WR018i005p01311.

Bradford, J.M., Ferris, J.E. and Remley, P.A. (1987), "Interrill soil erosion processes: I. effect of surface sealing on infiltration, runoff, and splash detachment", *Soil Sci. Soc. Am. J.*, **51**(6), 1566-1571. https://doi.org/10.2136/sssaj1987.03615995005100060029x.

Dunne, T., Zhang, W. and Aubry, B.F. (1991), "Effects of rainfall, vegetation, and microtopography on infiltration and runoff", *Water Resour. Res.*, **27**(9), 2271-2285. https://doi.org/10.1029/91WR01585.

Foley, J.L. and Silburn, D.M. (2002), "Hydraulic properties of rain impact surface seals on three clay soils - influence of raindrop impact frequency and rainfall intensity during steady state", *Aust. Soil Res.*, **40**(7), 1069-1083. https://doi.org/10.1071/SR01112.

Hawke, R.M., Price, A.G. and Bryan, R.B. (2006), "The effect of initial soil water content and rainfall intensity on near-surface soil hydrologic conductivity: A laboratory investigation", *Catena*, **65**(3), 237-346. https://doi.org/10.1071/SR01112.

Kim, S.K., Hong, W.P. and Kim, Y.M. (1991), "Prediction of rainfall-triggered landslides in Korea", *Proceedings of the International Symposium on Landslides*, Christchurch, New Zealand, February.

Leonard, J. and Andrieux, P. (1998), "Infiltration characteristics of soils in Mediterranean vineyards in Southern France", *Catena*, **32**(4), 209-223. https://doi.org/10.1016/S0341-8162(98)00049-6.

Lu, N. and Griffiths, D.V. (2004), "Profiles of steady-state suction stress in unsaturated soils", *J. Geotech. Geoenviron. Eng.*, **130**(10), 1063-1076. http://doi.org/10.1061/(ASCE)1090-0241(2004)130:10(1063).

Mahmood, K., Ryu, J.H., and Kim J.M. (2012), "Effect of anisotropic conductivity on suction and reliability index of unsaturated slope exposed to uniform antecedent rainfall", *Landslides*, **10**(1), 1-15. http://doi.org/10.1007/s10346-012-0325-9.

McIntyre, D.S. (1958), "Permeability measurements of soil crusts formed by raindrop impact", *Soil Sci.*, **85**(4), 85-189.

Mein, R.G. and Larson, C.L. (1973), "Modeling infiltration during a steady rain", *Water Resour. Res.*, **9**(2), 384-374. http://doi.org/10.1097/00010694-195804000-00002.

Morin, J. and Benyamini, Y. (1977), "Rainfall infiltration into bare soils", *Water Resour. Res.*, **13**(5), 813-817. https://doi.org/10.1029/WR013i005p00813.

Mwendera, E.J. and Feyen, J. (1994), "Effects of tillage and rainfall on soil surface roughness and properties", *Soil Technol.*, **7**(1), 93-103. https://doi.org/10.1016/0933-3630(94)90010-8.

Ojha, R., Corradini, C., Morbidelli, R. and Govindaraju, R.S. (2017), "Effective saturated hydraulic conductivity for representing field-scale infiltration and surface soil moisture in heterogeneous unsaturated soils subjected to rainfall events", *Water*, **9**(2), 134. https://doi.org/10.3390/w9020134.

Ören, A.H., Aksoy, Y.Y., Önal, O. and Demirkiran, H. (2018), "Correlating the hydraulic conductivities of GCLs with some properites of bentonites", *Geomech. Eng.*, **15**(5), 1091-1100. https://doi.org/10.12989/gae.2018.15.5.1091.
Park, K.B., Chae, B.G. and Park, H.J. (2011), "Analysis of rainfall infiltration velocity in unsaturated soils under both continuous and repeated rainfall conditions by an unsaturated soil column test", *J. Eng. Geol.*, **21**(2), 133-145. https://doi.org/10.9720/kseg.2011.21.2.133.
Philip, J.R. (1957), "The theory of infiltration: 1. The infiltration equation and its solution", *Soil Sci.*, **83**(5), 329-357. http://doi.org/10.1097/00010694-200606001-00009.
Poesen, J. (1984), "The influence of slope angle on infiltration rate and Hortonian overland flow", *Z. Geomorphol. Suppl. Bd.*, **49**, 117-131.
Poesen, J., Ingelmo-Sanchez, F. and Mucher, H. (1990), "The hydrological response of soil surfaces to rainfall as affected by cover and position of rock fragments in the top layer", *Earth Surf. Proc. Land.*, **15**(4), 653-671. https://doi.org/10.1002/esp.3290150707.
Romkens, M.J.M., Baumhardt, R.L., Parlange, M.B., Whisler, F.D., Parlange, J.Y. and Prasad, S.N. (1986), "Rain-induced surface seals: Their effect on ponding and infiltration", *Ann. Geophys.*, **4**(4), 417-424.
Schindewolf, M. and Schmidt, J. (2012), "Parameterization of the EROSION 2D/3D soil erosion model using a small-scale rainfall simulator and upstream runoff simulation", *Catena*, **91**, 47-55. https://doi.org/10.1016/j.catena.2011.01.007.
Song, Y.S, Hong, W.P. and Woo, K.S. (2012a), "Behavior and analysis of stabilizing piles installed in a cut slope during heavy rainfall", *Eng. Geol.*, **129-130**, 56-67, https://doi.org/10.1016/j.enggeo.2012.01.012.
Song, Y.S., Hwang, W.K., Jung, S.J. and Kim, T.H. (2012b), "A comparative study of suction stress between sand and silt under unsaturated condition", *Eng. Geol.*, **124**(4), 90-97. https://doi.org/10.1016/j.enggeo.2011.10.006.
Valentin, C. and Bresson, L.M. (1992), "Morphology, genesis and classification of surface crusts in loamy and sandy soils", *Geoderma*, **55**(3-4), 892-898. https://doi.org/10.1016/0016-7061(92)90085-L.
van Genuchten, M.T. (1980), "A closed-form equation for predicting the hydraulic conductivity of unsaturated soils", *Soil Sci. Soc. Am. J.*, **44**(5), 892-898. https://doi.org/10.2136/sssaj1980.03615995004400050002x.
Wilson, G.V. and Luxmoore, R.J. (1988), "Infiltration, macroporosity, and mesoporosity distributions on two forested watersheds", *Soil Sci. Soc. Am. J.*, **52**(2), 329-335. https://doi.org/10.2136/sssaj1988.03615995005200020005x.
Zhan, T.L.T., Jai, G.W., Chen, Y.M., Fredlund, D.G. and Li, H. (2013), "An analytical solution for rainfall infiltration into an unsaturated infinite slope and its application to slope stability analysis", *Int. J. Numer. Anal. Meth. Geomech.*, **37**(12), 1737-1760. https://doi.org/10.1002/nag.2106.

JS